RSC Advances

PAPER

View Article Online
View Journal | View Issue

Cite this: *RSC Adv.*, 2025, **15**, 35642

Characterization and antibacterial effect of green-synthesised silver nanoparticles using different extraction methods from *Ziziphus spina-christi* (Sidr) leaf extract collected from Syria

Wael Dagher,†[a] Abeer Alassod, †*[a] Mhd Firas Al Hinnawi,[b] Ibrahim Alghoraibi,[c] Amal Taher[d] and Manal Alnhlaoui[e]

Received 19th July 2025
Accepted 22nd September 2025

DOI: 10.1039/d5ra05214a

rsc.li/rsc-advances

The study investigates the effective green biosynthesis of silver nanoparticles (AgNPs) from silver nitrate ($AgNO_3$) as a precursor using Syrian Sidr leaf extract as a reducing and stabilizing agent. Three extraction methods (Maceration, ultrasound-assisted, and Soxhlet) were tested using six solvents. The Soxhlet method with a methanol/water mixture (60 : 40) provided the highest phenolic (192.83 ± 0.3 mg g^{-1}) and flavonoid (59.48 ± 7.45 mg g^{-1}) yields and was selected for nanoparticle biosynthesis. Further characterization confirmed the synthesis using these analytical techniques. UV-Vis spectroscopy revealed the formation of ZL-AgNPs *via* a characteristic plasmon resonance peak at 430 nm; FTIR indicated surface functional groups from the plant extract; XRD confirmed a cubic crystalline structure with an average crystallite size of 11 nm; SEM images showed spherical particles below 20 nm; EDX analysis depicted a dominant silver signal (85 wt%) with minor contributions from organic compounds. The biosynthesised ZL-AgNPs exhibited significant antibacterial activity against Gram-positive bacterium *Staphylococcus aureus* and the Gram-negative bacterium *Escherichia coli*, with inhibition zones ranging from 13.76 ± 0.25 to 21.65 ± 0.34 mm for *E. coli* and 0 to 16.73 ± 0.21 mm for *S. aureus* at concentrations of 25–200 μg mL^{-1}. The positive control (Gentamicin, 200 μg mL^{-1}) showed the largest inhibition zones, while the plant extract control demonstrated moderate activity at higher concentrations. These findings confirm the distinctive physicochemical properties and strong antibacterial potential of ZL-AgNPs for prospective biomedical applications.

1. Introduction

Due to high cost, immunogenicity, low bioavailability, and various other challenges associated with synthetic drugs, plant extracts have been extensively employed in medical materials. The growing concerns highlight the urgent need for safer, sustainable, and cost-effective alternatives, especially for communities with limited access to advanced healthcare systems.[1] Moreover, there is a pressing need for bioactive compounds derived from medicinal plants. Plant extracts are considered safe in biomedicine and pharmaceutics.

Medicinal plants have long been used as a natural source of treatments such as wound healing, burn management, fever reduction, and dyeing.[2–4] This form of medicine was historically called herbal medicine or traditional medicine. In recent decades, technological advancements in phytochemical analysis have not only validated many traditional uses but also revealed new pharmacological potentials, thus bridging ancient knowledge with modern medicine.[5,6] Recent technological advancements and a deeper understanding of plant chemistry have brought awareness of plant-derived medicinal compounds, playing a crucial role in drug development and enhancing treatment efficacy.[7]

Moreover, many modern pharmaceuticals contain naturally derived compounds obtained from plants such as opium poppy, cinchona, and Sidr or chemically synthesized analogs of these compounds.[8–10] Furthermore, Sidr is one of the most widely used medicinal plants in the middle east.[11] These species have been regarded as valuable medicinal resources for centuries due to their remarkable health benefits. Sidr belongs to the *Ziziphus* family, which includes various species and subspecies. Ongoing research highlights the medical significance of Sidr, with its

[a]*Textile Industries Mechanical Engineering and Techniques Department, Faculty of Mechanical and Electrical Engineering, Damascus University, Damascus, Syria. E-mail: abeeralassod@outlook.com*

[b]*Biomedical Engineering Department, Faculty of Mechanical and Electrical Engineering, Damascus University, Damascus, Syria*

[c]*Physics Department, Faculty of Science, Damascus University, Damascus, Syria*

[d]*Arab International University, Daraa, Syrian Arab Republic*

[e]*Plant Biology Department, Faculty of Science, Damascus University, Damascus, Syria*

† These authors contributed equally.

primary applications including anti-inflammatory treatments, diabetes management, antibacterial effects, wound and burn healing, and numerous other therapeutic uses. These benefits stem from its rich composition of essential bioactive compounds, including flavonoids, phenolics, alkaloids, saponins, and other phytochemicals.[12,13]

The emergence of nanotechnology has revolutionized various scientific fields, influencing material properties by altering their structure at the nanoscale and enabling their use in diverse applications.[14,15] This has led to developing various methods for synthesizing metallic nanoparticles, categorized into two main approaches: "top-down" and "bottom-up" methods. These include thermal decomposition, chemical and physical methods, and more advanced techniques like sonication and microwave-assisted synthesis.[16,17] Plant-based synthesis has gained significant attention in nanoparticle production. Biological synthesis using plant extracts is now recognized as an effective, cost-efficient, and environmentally friendly approach for producing metallic nanoparticles.[18–20] Nanoparticles have demonstrated extensive applications across various fields, with silver nanoparticles (AgNPs) standing out for their significant medical potential. AgNPs have been widely utilized in antibacterial and antimicrobial applications, drug delivery, and biosensing owing to their biocompatibility and non-cytotoxic properties. This makes them a safer option for pharmaceutical applications. The green synthesis of silver nanoparticles has been reported from various medicinal plants, including *Ziziphus*, as reducing, stabilizing, and capping agents in nanoparticle formation.[21–23] There are numerous biological, chemical, and physical methods for synthesizing metallic nanoparticles; however, biological methods have gained significant attention as they encompass environmentally friendly approaches that are non-toxic to living organisms and do not involve harmful or hazardous chemicals or radiation.[24–26] Biological methods rely on natural sources for nanoparticle preparation, such as plant parts (roots, flowers, and leaves), microorganisms, and enzymes, which makes them a unique approach for producing and synthesizing metallic nanoparticles (NPs) with various nanoscale shapes and sizes, without additional costs or the use of hazardous and toxic chemicals.[27–29]

One of the drawbacks of conventional methods for synthesizing metallic nanoparticles is low productivity and the potential hazards associated with the preparation process. Therefore, it is essential to adopt eco-friendly approaches, as they are more effective, less harmful to the environment, and applicable in various medical fields.[30] In recent years, interest has increased in the use of green synthesis of nanoparticles through plant extracts, as it represents an environmentally friendly and biologically safe alternative. *Ziziphus spina-christi* extract is considered a promising source, as it contains phenolic compounds and other bioactive substances capable of acting simultaneously as reducing and stabilizing agents during the preparation of metallic nanoparticles. Several studies have demonstrated its biological potential; for instance, Hussein *et al.*[31] reported that silver nanoparticles synthesized from this plant exhibited significant activity against resistant bacterial strains, with the potential to enhance the effects of certain conventional drugs. Similarly, Shnawa *et al.*[32] demonstrated that zinc oxide nanoparticles prepared using *Ziziphus* leaves showed antibacterial and antifungal activities, thereby reinforcing their potential applications in medical and environmental fields. On the other hand, Nazimuroya *et al.*[33] studied that saponin-containing nanoparticles derived from *Ziziphus* can be used as targeted drug carriers against cancer cells, while minimizing harm to healthy cells, thus opening new horizons for the utilisation of this plant in drug delivery systems.

However, despite the vast literature on green synthesis of AgNPs, there remains a clear research gap in investigating the optimal extraction methods for maximizing bioactive yield from Syrian Sidr leaves and linking these methods directly to nanoparticle synthesis efficiency and antibacterial performance.[34] In this study, we focus on the biosynthesis of silver nanoparticles using Syrian Sidr leaf extract. Various extraction techniques were employed, including ultrasound-assisted extraction (UAE), Soxhlet extraction, and traditional Maceration, using different solvents of varying polarities—ethanol, acetone, methanol, water, and their mixtures. By integrating the concepts of medicinal plant importance, nanotechnology potential, and eco-friendly synthesis, this study addresses both the scientific need for optimised nanoparticle synthesis and the practical demand for affordable biomedical solutions in resource-limited regions. This explores the potential of plant-based synthesis for producing metallic nanoparticles and evaluating their antibacterial properties.

This research aims to establish an optimised approach by comparing various extraction techniques and solvents to identify the most effective method for obtaining high-yield bioactive plant extracts. The ultimate goal is to achieve the most efficient synthesis of silver nanoparticles and evaluate their antibacterial potential.

2. Materials and methods

2.1. Plant and chemical materials

This study used Sidr leaves (*Zizyphus spina-Christi*), which grow in Syria. Leaves were collected in October 2023. The samples were collected from Sheikh Badr village in Tartus Governorate, Syria, an area encompassing natural protected zones containing *Ziziphus spina-christi* (Sidr) trees. The required solvents for the extraction process were as follows: Acetone (SHAM LAB, Extra pure), Absolute Ethanol 100% (VWR-CHEMICAL), Methanol (SHAM LAB, Extra pure), Silver Nitrate (ALFA CHEMICAL), Sodium Carbonate (SIGMA-ALDRICH), Sodium Hydroxide 99% Pure (TITAN BIOTECH LTD), Aluminium Chloride (RECTAPUR), Folin–Ciocalteu reagent 2M (SIGMA-ALDRICH), Sodium Nitrate (Citreos, Extra pure), Gallic Acid (QualiKems), and Quercetin (Metagenics). Deionized water and distilled water were also used. The tested bacterial strains were obtained from the Faculty of Science at Damascus University.

2.2. Preparation of plant extract from Sidr leaves

The gathered Sidr leaves were washed thoroughly with tap water, followed by several washes with distilled water to remove

dirt and dust. They were then air-dried until completely dehydrated and stored in a dark environment for two weeks until fully dried. After that, the leaves were crushed into a fine powder using an electric blender. The plant extraction was prepared using three different methods as follows:

2.2.1. Maceration method. In this method, finely cut and dried leaves (10 g) were ground and added to 100 mL of the solvent and left in the dark for three days. Maceration involves soaking the ground plant material in an appropriate amount of solvent at room or relatively low temperatures for a specified period, with occasional stirring. This allows soluble compounds to move from inside the plant cells into the solvent due to concentration gradients, making it a simple and effective method, particularly for heat-sensitive compounds. The extract was then filtered, centrifuged, and re-filtered using filter paper to remove residues. The solvent was recovered, and the extract was dried using a rotary evaporator to obtain a fine powder. The process was performed in two stages, and then the final dry extract was stored at 4 °C for further use. Scheme 1 depicts the Maceration process for Sidr leaves.

2.2.2. Soxhlet extraction method. Soxhlet extraction was performed using 10 g of dried and finely ground plant material, corresponding to 10% (w v^{-1}) of the extraction solvent. The plant material was placed in a cellulose extraction thimble inside the Soxhlet apparatus, as shown in Scheme 2. This technique operates on the principle of continuous hot solvent percolation: the solvent is boiled, evaporated, and condensed, allowing it to repeatedly wash over the plant material and dissolve target compounds until maximum extraction is achieved. The process was conducted at the solvent's boiling temperature for six hours with continuous reflux and solvent recycling. Six different solvents or solvent mixtures were used: ethanol, acetone, ethanol/acetone, ethanol/water, water, and methanol/water. The concentrated extracts were obtained under reduced pressure at 40 °C using a rotary evaporator to prevent thermal degradation of phenolic compounds. The dried crude extracts were stored at 4 °C in airtight containers. Six hours Soxhlet extraction time was selected, as the extraction yield increases during the initial period and plateaus thereafter.[35] The Soxhlet apparatus used in this study was located at the Faculty of Environmental Sciences, Latakia, Syria.

2.2.3. Ultrasound-assisted extraction method. 10 grams of plant material were added to 100 mL of solvent for each type of solvent used. The extraction was performed using an ultrasonic bath device (Jeken (CD/PS series), China) for 60 minutes at a frequency of 40 kHz, while maintaining a constant temperature of 40 °C to preserve the active compounds. Ultrasonic extraction uses high-frequency sound waves transmitted through a water bath containing the solvent and plant material. These vibrations help break down the plant tissue and increase the contact between the solvent and the bioactive compounds, thereby speeding up the extraction process and improving its

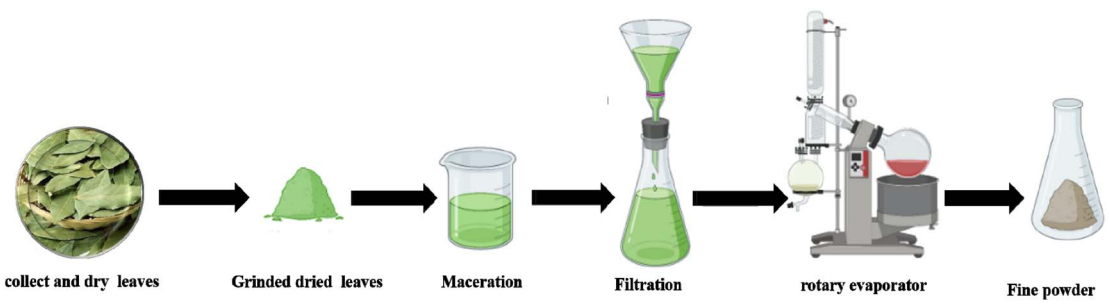

Scheme 1 Stages of Maceration method for Sidr leaves.

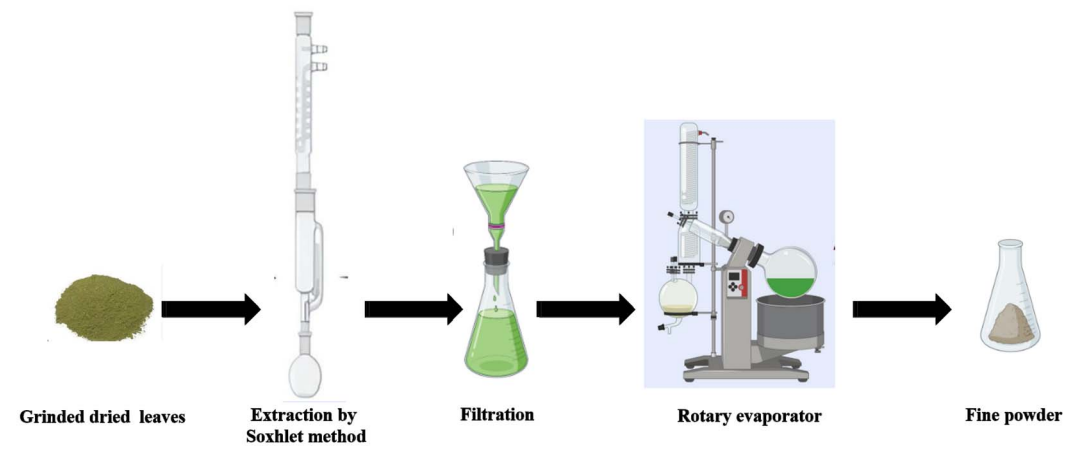

Scheme 2 Stages of the Soxhlet extraction method for Sidr Leaves.

efficiency, while preserving heat-sensitive compounds by operating at relatively low temperatures. The extract was then filtered and prepared for drying using a rotary evaporator to obtain the dry powder, which was stored at 4 °C until further use. Various solvents were used in the plant extract preparation, as outlined in Table 2. The average dry extract weight and extraction yield for each solvent were determined using the following equation:

$$E\% = (M/M_0) \times 100\% \quad (1)$$

where $E\%$: extraction efficiency, M: average sample weight (grams), M_0: total weight of plant material (grams).

2.3. Biosynthesis of silver nanoparticles and optimization of mixing ratios

Silver nitrate was used as a precursor for synthesising silver nanoparticles using Sidr leaves extract. The most effective solvent and extraction method were determined by identifying the highest concentration of key bioactive compounds in the plant extract. 10 g of plant extract was prepared by mixing a methanol/water solvent system (60 : 40) *via* Soxhlet extraction. The extract was then centrifuged and filtered according to the method outlined in the study[36] for nanoparticle synthesis. Varying amounts of silver nitrate were dissolved in 100 mL of deionized water in a beaker under magnetic stirring. The following silver nitrate concentrations were used in the synthesis process: 2 mM, 4 mM, 6 mM, and 8 mM, with different extract-to-silver nitrate ratios (20/80, 40/60, 60/40, and 80/20). The reaction was conducted at a temperature range of 40–50 °C for 15–20 minutes, under moderate pH conditions, and with continuous magnetic stirring at 400 rpm. The plant extract was added dropwise, and the appearance of a dark brown colour indicated the successful formation of silver nanoparticles. The reaction mixture was kept in the dark for 24 hours, followed by centrifugation at 10 000 rpm for 10 minutes. The obtained nanoparticles were washed multiple times and dispersed in acetone during the final wash. The nanoparticles were then dried in an oven (Memmert GMBH, Germany) at 50 °C for 48 hours, ground into a fine powder, weighed, and stored for further testing and applications. After synthesizing silver nanoparticles, UV-Visible spectrophotometry (UV-Vis) was performed to determine the optimal silver nitrate concentration. Based on the obtained spectra, the best silver nitrate concentration was selected for further optimization of mixing ratios between the plant extract and silver nitrate (20 : 80, 40 : 60, 60 : 40, 80 : 20). The same verification procedure was followed to determine the most effective ratio for further characterization.

3. Characterization of silver nanoparticles

3.1. Fourier Transform Infrared spectroscopy (FTIR)

The functional groups and chemical compounds involved in synthesising silver nanoparticles were investigated with FTIR spectroscopy (Jasco FTIR 4200 spectrometer, Japan). The analysis was conducted by scanning the sample with infrared radiation in the range 400–4000 cm^{-1} at a resolution of 4 cm^{-1}.

3.2. UV-Visible spectroscopy (UV-Vis)

The structural composition of the silver nanoparticles was monitored by identifying their characteristic wavelengths of absorption using UV-Vis spectra (Varian Cary 5000 UV-Vis spectrophotometer, USA). This method involved directing a light beam over a specific wavelength range to detect the formation of silver nanoparticles. The spectral measurements were conducted within a 200–800 nm wavelength range and 1 nm resolution.

3.3. Scanning electron microscopy (SEM)

SEM was used to analyze the morphology and surface structure of the synthesized silver nanoparticles. The analysis was conducted using SEM (TESCAN VEGA, Czech Republic) at magnifications ranging from 20 kx to 100 kx. The samples were fixed on the tubular aluminium stub with double-sided tape. The stub-supported samples were coated with gold. Finally, the gold-coated samples were placed under the microscope to observe the morphology.

3.4. X-ray diffraction (XRD)

To determine the crystalline structure of the silver nanoparticles, X-ray diffraction (XRD) (STADI Germany) was employed. This technique provided essential information about the nanoparticles by analyzing diffraction patterns of X-ray radiation at scanning angles ranging from 10° to 80°, with a 40 kW radiation source. The analysis helped to determine key crystallographic parameters, such as crystallinity degree, crystallite size, and lattice structure. The instrument model used for XRD analysis was (STOE).

3.5. Energy dispersive X-ray spectroscopy (EDX)

EDX analysis was performed to determine the elemental composition of the synthesized silver nanoparticles. This technique relies on the excitation of the sample using a high-energy electron beam, which causes the emission of characteristic X-rays specific to the elements present. The analysis provided data on the atomic and weight percentages of the elements in the sample, offering insight into the composition and purity of the synthesized nanoparticles. The EDX system was integrated with the TESCAN VEGA/SEM microscope.

3.6. Determination of antibacterial activity

The antibacterial activity of the synthesized silver nanoparticles was evaluated against a Gram-negative and Gram-positive bacterial strain by measuring the inhibition zone at different nanoparticle concentrations compared to a conventional antibiotic. The test was conducted using *E. coli* and *S. aureus* through the well diffusion method on an agar plate. A sterilized blank disc was placed, wells were created, and an equal volume of test materials was added. The antibacterial activity of silver nanoparticles synthesized from Sidr extract was assessed by

incubating the plates at 37 °C for 24 hours and measuring the inhibition zone diameter in (mm) as the bacterial strains used were clinically isolated. Different concentrations of the synthesized silver nanoparticles (50, 100, 150, and 200 μg mL^{-1}) were tested to determine the inhibition zone. These concentrations were used to evaluate the inhibition of bacterial growth based on the diameter of inhibition zones, providing insights into the effectiveness of silver nanoparticles against these bacteria. The test was performed by inoculating the bacterial strain onto agar plates, adding 50 μL of the test sample into each well, and incubating the plates at 37 °C for 24 hours. Three replicates were conducted for each concentration. The inhibition zone was measured using ImageJ software.

3.7. Phytochemical analysis

3.7.1. Determination of total phenolic content (TPC) in Sidr leaf extract. The total phenolic content was evaluated using the method described in,[37] with minor modifications. 1 mg of the dried extract was dissolved in 1 mL of 70% methanol in test tubes for each solvent and extraction method used in the study. The solution was left in a dark environment for 24 hours with intermittent stirring to ensure complete dissolution. The mixture was then centrifuged at 8000 rpm for 10 minutes, filtered, and stored at 4 °C. For analysis, 400 μL of the prepared solution was placed in a sterile heated tube, followed by adding 2.5 mL of 10% Folin–Ciocalteu reagent. The mixture was left in the dark for 5 minutes, then 2 mL of 5% sodium carbonate was added, and the tubes were shaken continuously before incubation in the dark for 1 hour. The absorbance was measured at 765 nm, and three readings were taken for each sample. The total phenolic content was calculated using the following equation and expressed as mg of gallic acid per g of dry extract:

$$\mathrm{TPC} = C \times (V/M) \quad (2)$$

where TPC: total phenolic content (mg GA per g dry extract), C: gallic acid equivalent concentration from the standard curve (μg mL^{-1}), V: extract volume (mL), M: extract weight (g).

3.7.2. Standard curve for total phenolic content estimation. A gallic acid standard curve was prepared as a reference for determining total phenolic content. A 300 μg mL^{-1} stock solution of gallic acid was diluted into a standard series of 18.75, 37.5, 75, and 150 μg mL^{-1} in methanol. The gallic acid solution was prepared following the same method as the plant extract and measured at 765 nm. The standard curve slope was used to estimate the total phenolic content in Sidr leaf extract.

3.7.3. Determination of total flavonoid content (TFC) in Sidr leaf extract. The total flavonoid content was determined using a method similar to the phenolic content analysis, with modifications. The dried extract was dissolved in water and prepared in the same manner as the previous extraction method. The total flavonoid content was determined according to the procedure described. The prepared plant extract (5 mL) was combined with 0.3 mL of 6% sodium nitrate and incubated in complete darkness for 6 minutes. In the next step, 0.3 mL of 10% aluminium chloride was added, followed by 5 minutes of incubation in the dark. Finally, 2 mL of 5% sodium hydroxide was added, and the total volume was adjusted with distilled water.

After incubation for 1 hour in the dark, the absorbance was measured at 515 nm. Three readings were recorded per sample, and the total flavonoid content was calculated as mg of quercetin per g of dry extract (mg Q per g dry extract) using the following equation:

$$\mathrm{TFC} = C \times (V/M) \quad (3)$$

where TFC: total flavonoid content (mg Q per g dry extract), C: quercetin equivalent concentration from the standard curve (μg mL^{-1}), V: extract volume (mL), M: extract weight (g).

3.7.4. Standard curve for total flavonoid content estimation. A quercetin standard curve was prepared by diluting a 300 μg mL^{-1} quercetin stock solution into a standard series of 18.75, 37.5, 75, and 150 μg mL^{-1}. The solution was prepared as described earlier and measured at 515 nm. The standard curve slope was used to estimate the total flavonoid content in *Zizyphus spina-Christi* leaf extract.

3.8. Statistical analysis

Data analysis was performed using SPSS software, version 26. A two-way analysis of variance (Two-way ANOVA) was applied to estimate both the individual and interactive effects of the studied factors on the measured parameters. The inhibition zone diameters were measured by taking two perpendicular diameters for each zone, followed by calculating the mean value, and then averaging across the three replicates for each concentration. The differences in antibacterial activity among the tested groups (silver nanoparticles at different concentrations) were evaluated using one-way analysis of variance (ANOVA), followed by Duncan's post hoc test to determine significant differences between means. Pearson correlation analysis was conducted to assess the strength and direction of the relationship between total flavonoid content, total phenolic content, and extraction yield, and antibacterial activity. Statistical significance was determined at $P > 0.05$, and Tukey's HSD test was used for post-hoc comparisons among means.

4. Results and discussion

In this study, several extracts derived from *Ziziphus* plant leaves were prepared using various preparation methods and solvents for the synthesis of silver nanoparticles. Plants belonging to the *Ziziphus* genus contain high levels of bioactive compounds such as phenolics and flavonoids, which play a role in antibacterial, antifungal, and antioxidant applications. Many studies have referenced the use of different parts of the *Ziziphus* plant, but there is limited information on a comprehensive comparison of extraction and preparation methods.

4.1. Extraction (different methods and media) and extraction efficiency

Three different extraction methods were adopted (Soxhlet extraction, ultrasound-assisted extraction, and traditional

Maceration extraction). At the same time, a wide range of solvents and their mixtures were used. The solvents included (water, ethanol, and acetone) in pure concentrations, and the mixtures were in a 60/40 ratio (ethanol/water, ethanol/acetone, methanol/water). Various methods and solvents were used to determine the best and most effective method for preparing silver nanoparticles. Safety and precautionary measures were considered to minimize risks associated with the materials and equipment used in the preparation process. The results indicated that both the extraction methods (Soxhlet, ultrasound, Maceration) and the type of solvent used (ethanol, acetone, ethanol/acetone, ethanol/water, water, methanol/water) had varying effects on the extraction yield from *Ziziphus* leaves. Although no statistically significant effect was observed for each variable independently ($P > 0.05$), the two-way ANOVA analysis demonstrated a cumulative interaction effect between the method and solvent on the yield (partial eta squared = high), indicating factor interactions.

Table 1 enlists the dry plant extract weight and extraction efficiency of the solvents used in the study for *Ziziphus* leaves. The extraction efficiency, used as a comparison criterion, ranged between 2.8% and 24.57% in different extraction methods. The lowest value was observed with ethanol as a solvent in ultrasound-assisted extraction, while the highest efficiency was achieved using an ethanol/water mixture in Soxhlet extraction. This indicates that several key factors significantly affect the extraction process, leading to variations in the bioactive compounds within the extract. These factors include the method, solvent, and combination of solvents.

When using the Soxhlet apparatus as an extraction method, the extraction efficiency of solvent mixtures was higher than that of pure solvents, except for water. The extraction efficiency followed the order (ethanol/water > water > ethanol/acetone > methanol/water > ethanol > acetone), with values of 24.59% > 16.7% > 12.23% > 6.21% > 3.95% > 3.39%, respectively. The high extraction yield is attributed to the physical effects associated with the extraction process, such as heat and the continuous soaking of the plant material in the solvent throughout the extraction period. This aligns with a study on the effect of extraction methods on the chemical composition and antioxidant activity of *L. Aerial*, which compared Soxhlet and cold Maceration methods. The study found that the highest extraction yield was obtained using Soxhlet with methanol as the solvent, explaining the differences in extraction conditions and duration between the two methods.[38]

Table 1 Extraction efficiency based on different methods and solvents for *Ziziphus* leaf extract

Method	Solvent	Weight(g)/20g	Yield%
Soxhlet extractor	Ethanol	0.79	3.95
Soxhlet extractor	Acetone	0.678	3.39
Soxhlet extractor	Ethanol/acetone	2.446	12.23
Soxhlet extractor	Ethanol/water	4.918	24.59
Soxhlet extractor	Water	3.34	16.7
Soxhlet extractor	Methanol/water	2.242	6.21
Ultra-sonic extractor	Ethanol	0.56	2.8
Ultra-sonic extractor	Acetone	0.598	2.99
Ultra-sonic extractor	Ethanol/acetone	1.4258	7.129
Ultra-sonic extractor	Ethanol/water	3.5	17.5
Ultra-sonic extractor	Water	2.35	11.75
Ultra-sonic extractor	Methanol/water	1.391	4.955
Maceration	Ethanol	1.834	9.17
Maceration	Acetone	1.4342	7.171
Maceration	Ethanol/acetone	1.815	5.575
Maceration	Ethanol/water	4.19	20.95
Maceration	Water	2.813	14.065
Maceration	Methanol/water	2.1276	10.638

Regarding ultrasound-assisted extraction, it exhibited the lowest extraction efficiency among the methods used in this study. The efficiency ranking for *Ziziphus* extraction was (ethanol/water > water > ethanol/acetone > methanol/water > acetone > ethanol), with values of 17.5% > 11.75% > 7.129% > 4.995% > 2.99% > 2.8%, respectively. This ranking was relatively similar to the previous extraction method, but with significantly lower values for the same dry plant material weight.

For the traditional Maceration method used to extract *Ziziphus* leaves, relatively high extraction efficiency values were observed. The ranking of efficiency based on different solvents was (ethanol/water > water > methanol/water > ethanol > acetone > ethanol/acetone), with values of 20.95% > 14.065% > 10.638% > 9.17% > 7.171% > 5.575%, respectively. Although the ranking remained consistent across different methods, ethanol/acetone extraction lagged slightly behind other solvents. This method relies on the soaking duration of the plant material in the solvent to obtain the dry extract. It has been reported that Maceration is less efficient than Soxhlet extraction due to differences in operational conditions, particularly temperature, which enhances extraction yield. The extraction yield was 8.7–12% for Maceration and Soxhlet methods, respectively, with the highest yield obtained using an ethanol/water mixture. The solvents followed the ranking ethanol/water > ethanol > water, which was also consistent for total phenolic content.[39,40] It was observed that Maceration using water or ethanol/water produced some of the highest yields, likely due to the prolonged soaking period (72 hours) compared to other methods, allowing sufficient time for the diffusion of soluble compounds. In contrast, the Soxhlet method showed remarkable effectiveness, particularly with organic solvents, due to stable temperature and continuous solvent dynamics.[41] On the other hand, the ultrasound method was time-efficient but could be limited if conditions were not adequately controlled, potentially causing excessive cell disruption.[42,43]

An apparent variation in extraction yield was observed when comparing the previous methods. Soxhlet extraction produced the highest yield using a methanol/water solvent, ranking the methods as Soxhlet > Maceration > ultrasound-assisted extraction. Despite the thermal impact of the Soxhlet method, it offers advantages such as extracting a higher concentration of bioactive compounds from a smaller plant material sample, without requiring filtration or centrifugation, unlike the other two methods. Additionally, solvent mixtures yielded a higher extraction output compared to pure solvents, except for water. A comparative study on extraction techniques and solvents for *Acacia dealbata* and *Olea europaea* extracts, using multiple solvents and methods, concluded that extraction efficiency is

closely related to the solvent used. Soxhlet and microwave-assisted extraction methods showed the highest efficiency.[44] Another study on the effect of extraction on bioactive compound content in medicinal extracts confirmed that solvent mixtures with water resulted in higher yields due to the dissolution of polar carbohydrates and glycosides from secondary metabolites.[45]

4.2. Phenolic and flavonoid content

Although bioactive compounds are found in all plant parts, their quantities vary due to factors such as environmental conditions, nutrition, and species differences within the same family. *Ziziphus*'s total phenolic and flavonoid content was measured using the previously mentioned methods and solvents, as outlined in Table 2. The total phenolic content was determined using the standard calibration curve of gallic acid, illustrated in Fig. 1, yielding the regression equation $Y = 0.0083X + 0.0004$ ($R^2 = 0.97$). Similarly, the total flavonoid content was determined using the standard calibration curve of quercetin, shown in Fig. 2, with the regression equation $Y = 0.0009X + 0.0010$ ($R^2 = 0.982$).

The tow-way ANOVA statistical analysis showed highly significant differences ($P < 0.001$) for all studied factors, with an F-value of 6832.140 (Eta squared = 0.997) for the extraction method, 497.409 (Eta squared = 0.986) for the solvent type, and 204.754 (Eta squared = 0.983) for their interaction. These values confirm that the studied variables collectively explain more than 98% of the total variance in the data, which agrees with the result of a study conducted by Zhang *et al.* on similar medicinal plant.[41] This study's TPC values were relatively high when using different solvents and extraction methods. Table 3 and chart (3) illustrate the variation in values when analyzing the total phenolic content, ranging from 95.84 ± 1.12 mg GAE per g to a maximum of 192.83 ± 0.3 mg GAE per g, which was achieved using the Soxhlet apparatus with a methanol/water solvent.

The highest TPC values were observed in the Soxhlet method, followed by Maceration and then Ultrasound. The superior performance of the Soxhlet method with methanol–water (60 : 40) which recorded the highest mean TPC (192.82 ± 3.14 mg GAE per g) according to the Tukey HSD test ($p < 0.001$)—is attributed to several mechanisms, including the temperature effect that facilitates the breakdown of hydrogen bonds between phenolic compounds and cellular structures, as demonstrated by Zhou *et al.* using spectroscopic techniques,[46] further confirmed regarding the efficiency of Soxhlet compared to the modern method.[47] Additionally, the methanol–water (60 : 40) mixture provides an optimal polarity balance for extracting a wide spectrum of compounds, which was confirmed by the systematic solvent study of El Hadrami *et al.*[48] Conversely, the weaker performance of ultrasound extraction can be attributed to the short extraction time, which is insufficient for extracting firmly bound phenolics, or to the degradation and oxidation of sensitive compounds, as recently documented using LC-MS analyses.[41] The intermediate performance of Maceration suggests limited efficiency in extracting medium-polarity phenolics, as described by Poojary *et al.*[49]

When comparing each solvent across different methods separately, absolute ethanol followed the order (Soxhlet > Maceration > Ultrasound), absolute acetone followed (Soxhlet > Maceration > Ultrasound), distilled water followed (Maceration > Soxhlet > Ultrasound), ethanol/acetone mixture followed (Maceration > Soxhlet > Ultrasound), ethanol/water mixture followed (Soxhlet > Maceration > Ultrasound). Methanol/water mixture followed (Soxhlet > Maceration > Ultrasound).

It was observed that ultrasound-assisted extraction ranked lowest in extracting total bioactive compounds, which the processing conditions, such as temperature and ultrasound

Table 2 Total phenolic content as a function of extraction method and solvent for the extract of Sidr leaves[a]

Method	Symbol	Solvent	MeanTPC (mg g^{-1})	Mean TPC ±SD (mg g^{-1})
Soxhlet extractor	1	Ethanol	181.07	181.08 ± 0.50^{a}
Soxhlet extractor	1	Acetone	168.91	168.51 ± 1.50^{b}
Soxhlet extractor	1	Ethanol/acetone	154.85	154.85 ± 1.50^{bc}
Soxhlet extractor	1	Ethanol/water	167.54	167.54 ± 1.12^{b}
Soxhlet extractor	1	Water	165.39	165.39 ± 1.18^{b}
Soxhlet extractor	1	Methanol/water	192.82	192.83 ± 0.3^{a}
Ultra-sonic extractor	2	Ethanol	114.31	114.31 ± 1.49^{d}
Ultra-sonic extractor	2	Acetone	95.84	95.84 ± 1.12^{e}
Ultra-sonic extractor	2	Ethanol/acetone	123.57	123.57 ± 1.55^{d}
Ultra-sonic extractor	2	Ethanol/water	110.47	110.47 ± 1.35^{d}
Ultra-sonic extractor	2	Water	120.84	120.84 ± 0.35^{d}
Ultra-sonic extractor	2	Methanol/water	132.80	132.80 ± 0.54^{cd}
Maceration	3	Ethanol	143.49	143.49 ± 1.67^{c}
Maceration	3	Acetone	120.35	120.35 ± 0.95^{d}
Maceration	3	Ethanol/acetone	157.22	157.22 ± 1.08^{bc}
Maceration	3	Ethanol/water	155.42	155.42 ± 0.99^{bc}
Maceration	3	Water	169.54	169.54 ± 1.74^{b}
Maceration	3	Methanol/water	156.97	156.97 ± 0.3^{bc}

[a] Different letters within the same column indicate significant differences at the level of ($P < 0.05$) according to the Tukey HSD test.

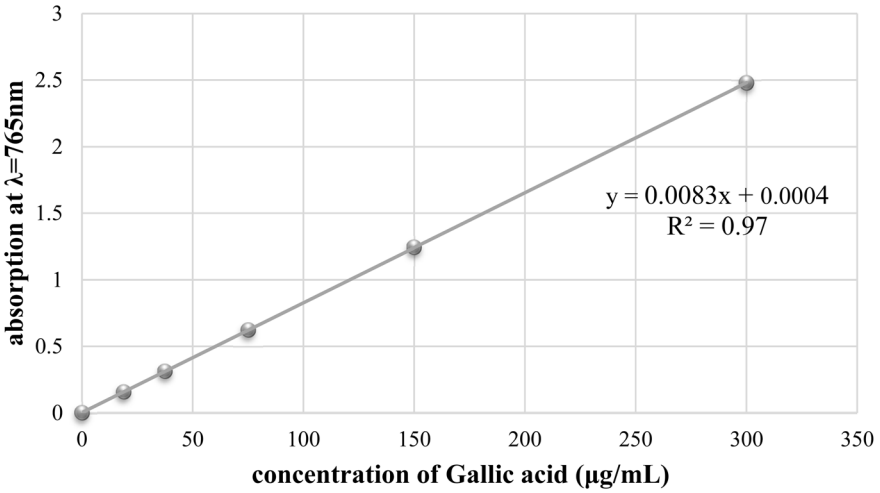

Fig. 1 The standard curve of gallic acid measured in (µg mL^{-1}).

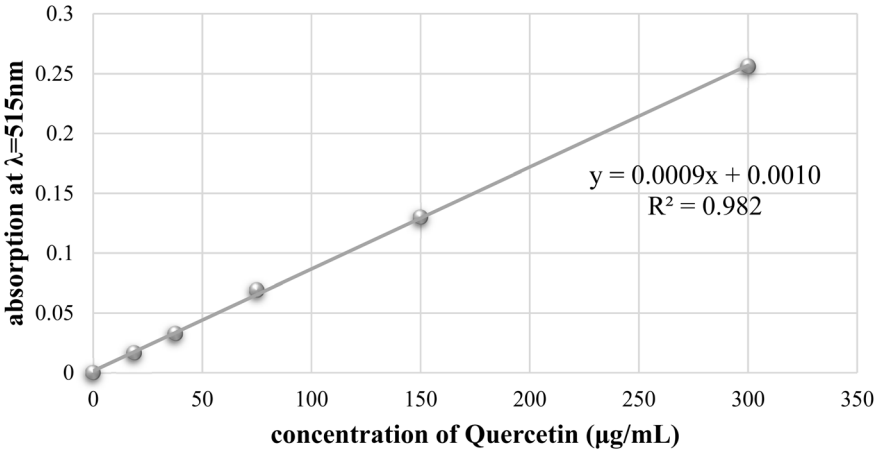

Fig. 2 The standard curve of quercetin measured in (µg mL^{-1}).

intensity, can explain. This finding aligns with reports on recent advancements and comparisons with traditional methods for phenolic compound extraction, confirming that bioactive compound yield depends on operational conditions when using ultrasound-assisted extraction and overall extraction efficiency.[50]

From the comparison of solvents mentioned above in Fig. 3 and Table 2, it can be observed that extraction using distilled water and a mixture of ethanol and acetone deviated from the ranking of the most effective methods. Although the values are very close, it can be stated that the Soxhlet method is unsuitable for efficiently extracting bioactive compounds from plants when using either of these solvents. This is because the method relies on continuous solvent evaporation. Since the boiling point of water is higher than that of other solvents, this leads to a relative degradation of the active compounds. Similarly, the ethanol-acetone mixture, which evaporates quickly, might cause partial degradation of the active compounds due to brief exposure to heat.

The lower values obtained with ethanol and acetone in ultrasonic extraction can be attributed to the shorter duration of ultrasound exposure compared to other methods, which are generally more effective due to differences in preparation conditions and the physical impact associated with the two alternative techniques. A study comparing the effects of extraction methods and solvents on the biological activities of chemical compounds from various flowers concluded that a mixture of water and methanol was the most suitable for extracting phenolic compounds. It exhibited 32% higher effectiveness when using a 70% solvent concentration.[45] Alara *et al.* confirmed the superiority of aqueous alcoholic solvents in extracting phenolics from *Ziziphus* compared to pure solvents,[51] which is attributed to the nature of the active compounds being extracted. These results align with the findings of Melek *et al.*, who reported that combining water with polar solvents such as methanol enhances the solubility and release of phenolic compounds from plant cells. Furthermore, water facilitates the disruption of hydrogen bonds and allows the liberation of compounds bound to proteins and carbohydrates.[52]

Table 3 Total flavonoid content as a function of extraction method and solvent for the extract of Sidr leaves[a]

Method	Symbol	Solvent	Mean TFC (mg g^{-1})	Mean TFC ±SD (mg g^{-1})
Soxhlet extractor	1	Ethanol	28.00	28.01 ± 0.58^{b}
Soxhlet extractor	1	Acetone	15.55	15.56 ± 0.84^{d}
Soxhlet extractor	1	Ethanol/acetone	15.037	15.04 ± 1.04^{d}
Soxhlet extractor	1	Ethanol/water	18.518	18.52 ± 0.76^{cd}
Soxhlet extractor	1	Water	14.748	14.75 ± 0.68^{d}
Soxhlet extractor	1	Methanol/water	59.48	59.48 ± 7.45^{a}
Ultra-sonic extractor	2	Ethanol	19.72	19.72 ± 0.91^{cd}
Ultra-sonic extractor	2	Acetone	14.369	14.37 ± 0.64^{d}
Ultra-sonic extractor	2	Ethanol/acetone	14.445	14.45 ± 0.61^{d}
Ultra-sonic extractor	2	Ethanol/water	25.545	25.55 ± 0.43^{bc}
Ultra-sonic extractor	2	Water	33.16	33.16 ± 0.90^{b}
Ultra-sonic extractor	2	Methanol/water	30.44	30.44 ± 1.11^{b}
Maceration	3	Ethanol	25.60	25.60 ± 0.61^{bc}
Maceration	3	Acetone	15.57	15.57 ± 0.35^{d}
Maceration	3	Ethanol/acetone	23.90	23.91 ± 0.49^{bc}
Maceration	3	Ethanol/water	26.98	26.98 ± 0.68^{bc}
Maceration	3	Water	15.449	15.45 ± 0.61^{d}
Maceration	3	Methanol/water	39.70	39.70 ± 0.67^{b}

[a] Different letters within the same column indicate significant differences at the level of ($P < 0.05$) according to the Tukey HSD test.

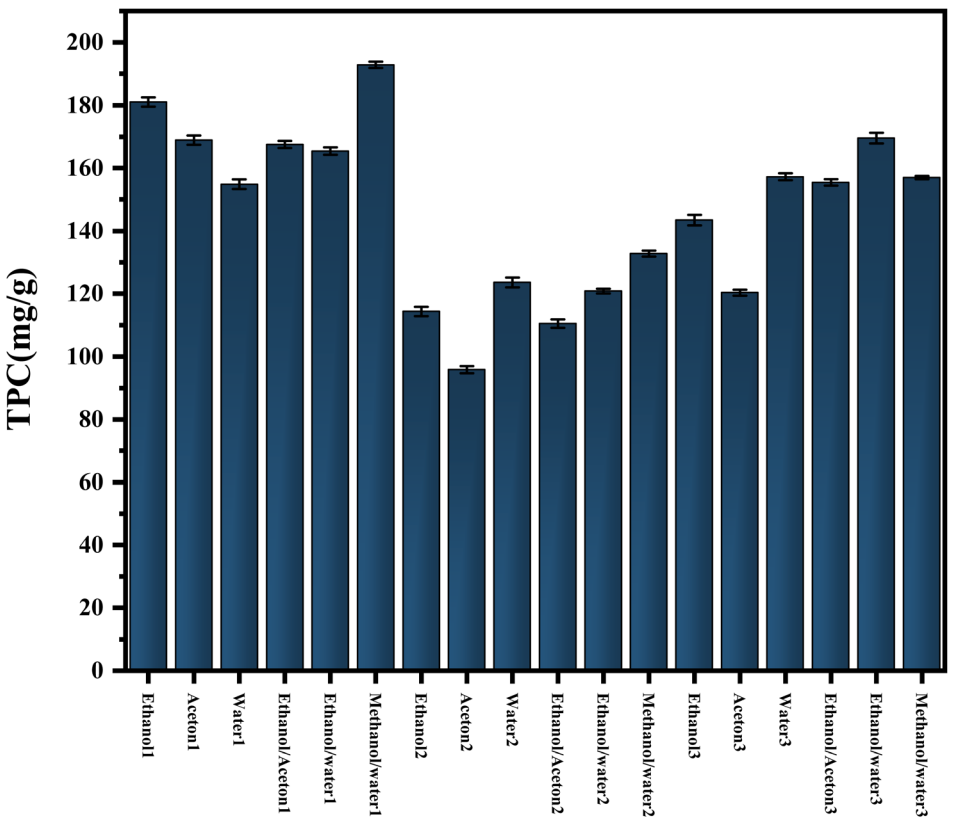

Fig. 3 Total phenolic content using different extraction techniques and selected solvents for the extract of Sidr leaves.

Ultimately, it can be noted that the highest value was achieved using a methanol/water mixture through the Soxhlet extraction method.

The results of the two-way ANOVA showed that both the extraction method and the type of solvent had a significant effect on the total flavonoid content extracted from *Ziziphus* leaves ($p < 0.05$). The impact of the extraction method was statistically significant ($p = 0.017$, partial Eta Squared = 0.202), where the Tukey HSD test revealed that Soxhlet yielded higher flavonoid quantities compared to ultrasound ($p = 0.015$). In

contrast, no significant difference was observed between Maceration and the other methods, despite noticeable numerical differences. As for the solvent effect, it was highly significant ($p = 0.000$, partial Eta Squared $= 0.958$), indicating that solvent selection is the most decisive factor in determining the amount of flavonoids extracted. The combined effect of both method and solvent was also highly significant ($p = 0.000$, partial Eta Squared $= 0.923$), suggesting that solvent effectiveness depends on the method used, and *vice versa*. The total flavonoid content (TFC) was determined as shown in Fig. 4 and Table 3, where the TFC values across different extraction methods and solvents ranged between 14.37 ± 0.64 mg Q per g and 59.48 ± 7.45 mg Q per g.

When comparing the methods, Soxhlet achieved relatively high values when appropriate solvents were applied. In contrast, ultrasound performance was lower in particular combinations, likely due to excessive cell wall disruption, which could allow the extraction of other compounds interfering with flavonoid analysis. Meanwhile, Maceration with ethanol/water or methanol/water showed favorable results,[53] indicating that longer extraction times allow greater recovery of soluble compounds without subjecting them to thermal stress. These findings are consistent with Li *et al.*, who emphasized that increased polarity and extended contact time between solvent and plant material are critical factors for improving flavonoid yield.[54] In contrast, non-polar solvents or mixtures with low water content reduced the yield. However, these results differ from some reports highlighting the superiority of pure ethanol or acetone, which may be attributed to differences in plant source, chemical composition, and experimental conditions.[55] Ultimately, the highest flavonoid content was obtained using the Soxhlet method with a methanol/water solvent for plant extract preparation. Additionally, these values were correlated with the total phenolic and flavonoid content. A previous study[38] indicated a similarity between the bioactive compound values obtained using the Soxhlet and Maceration methods. However, a significant difference was observed when methanol was used as the solvent, where the total flavonoid content reached 163.64 mg QE per g with the Soxhlet method, compared to 162.61 mg QE per g with the Maceration method.

Pearson's tests revealed that the correlation between phenolic and flavonoid content was moderate and significant ($r \approx 0.35$, $p < 0.05$), suggesting a partial similarity in extraction mechanisms or structural associations between the two compounds. However, the correlation between yield and active compound content was not significant, indicating that higher yield does not necessarily reflect increased phenolics or flavonoids, possibly due to the extraction of other compounds such as sugars or proteins.[8] The weak correlation can be explained by the fact that optimal conditions were applied for each method in terms of duration, which made the extraction efficiency of each compound category dependent on its specific interaction with time and temperature. As a result, the highest values of all components did not occur simultaneously in the same

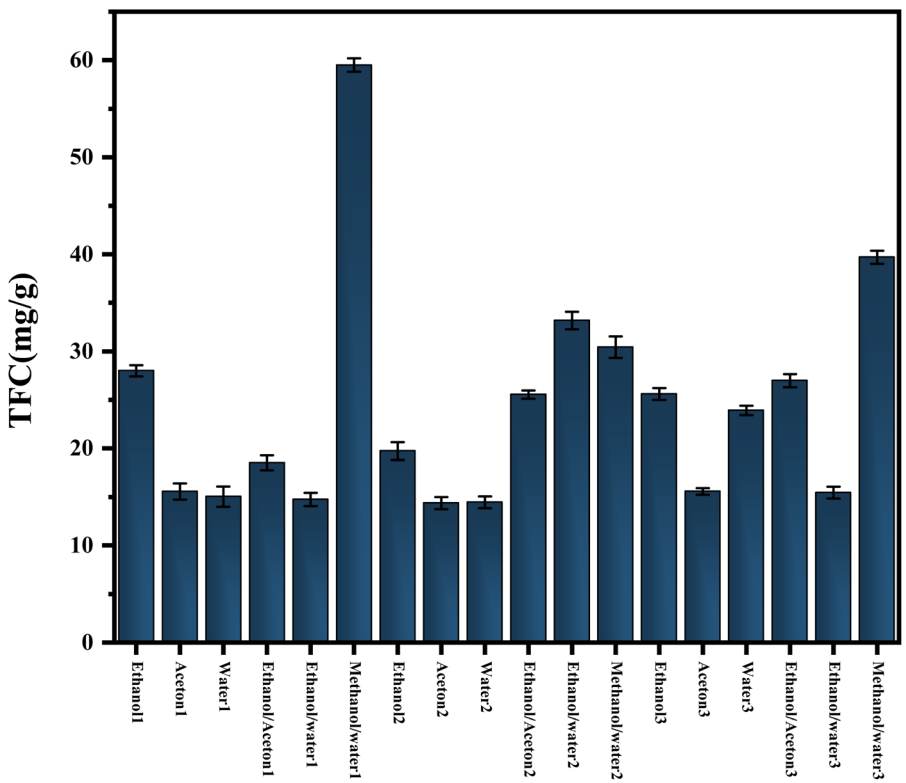

Fig. 4 Total flavonoid content using different extraction techniques and selected solvents for the extract of Sidr leaves. The total flavonoid content values using the Soxhlet method followed this order: methanol/water > ethanol > ethanol/water > acetone > ethanol/acetone > water. For the ultrasonic-assisted extraction method, the order was: water > methanol/water > ethanol/water > ethanol > ethanol/acetone > acetone. For Maceration extraction, the order was: methanol/water > ethanol/water > ethanol > ethanol/acetone > acetone > water.

treatment. Similar findings have been reported in studies for green tea, thyme, and other medicinal plants, where the correlation between yield and TPC/TFC was often weak or absent.[42,52]

4.3. Characterization of silver nanoparticles

4.3.1. UV-Visible spectral analysis (UV-Vis). UV-Visible absorption spectroscopy was used as a technique to characterize the green-synthesized silver nanoparticles (AgNPs) prepared using *Ziziphus* leaf extract in the wavelength range of 200–800 nm. The samples were prepared at the proposed silver nitrate concentrations (2-4-6-8 mM). The analysis was conducted using distilled water as the baseline, while the main sample was diluted and placed in a separate cuvette (3 mL volume) before being measured. The spectra of the tested samples were recorded and plotted using Origin V-22 software.

4.3.2. Effect of silver nitrate concentration. The concentration of silver nitrate ($AgNO_3$) significantly affects the nucleation, growth, and final characteristics of biosynthesized silver nanoparticles. In this study, the plant extract was obtained from *Ziziphus* leaves *via* Soxhlet extraction using a methanol/water (M/W) solvent mixture in a 40 : 60 ratio. Silver nanoparticles were synthesized at four different precursor concentrations (2, 4, 6, and 8 mM) while keeping all other parameters constant: temperature (40 °C), reaction time (30 min), and extract-to-silver nitrate ratio (80 : 20). As shown in Fig. 5, the UV-Visible spectra revealed that at lower $AgNO_3$ concentrations (2 and 4 mM), the surface plasmon resonance (SPR) absorption bands were broader, of lower intensity, and slightly red-shifted, indicating larger particle sizes and possible polydispersity as it listed in Table 4. When the concentration increased to 6 mM and 8 mM, the absorption peaks became sharper, narrower, and blue-shifted toward shorter wavelengths (430–440 nm), which is characteristic of smaller, more uniformly distributed nanoparticles due to enhanced nucleation rates.[56] The observed blue shift in the SPR peak is a direct consequence of the Mie theory, where smaller particle sizes cause higher resonance frequencies due to more coherent oscillation of conduction electrons on the nanoparticle surface. Increasing the precursor concentration enhances the availability of Ag^+ ions, leading to a higher number of nucleation sites and, thus, more nanoparticles in solution, which increases absorbance intensity.

However, beyond the optimal concentration (in this case, 8 mM), excess silver ions can cause uncontrolled growth and agglomeration, resulting in broader peaks and decreased absorbance.[57,58] These findings align with a previous study on the green synthesis of AgNPs using Vernonia amygdalina, which reported SPR peaks between 415–440 nm for concentrations ranging from 1 to 10 mM. Our results recorded a peak at 410 nm for similar concentrations, confirming the consistency of SPR behaviour with concentration changes. Based on these observations, the 8 mM $AgNO_3$ concentration was selected for further characterization, maintaining all other experimental conditions unchanged.

4.3.3. Effect of extract-to-silver nitrate ratio. The mixing ratio between silver nitrate solution and plant extract plays a crucial role in determining the size and yield of the synthesized silver nanoparticles. This ratio influences color variations and helps determine the optimal spectral conditions for

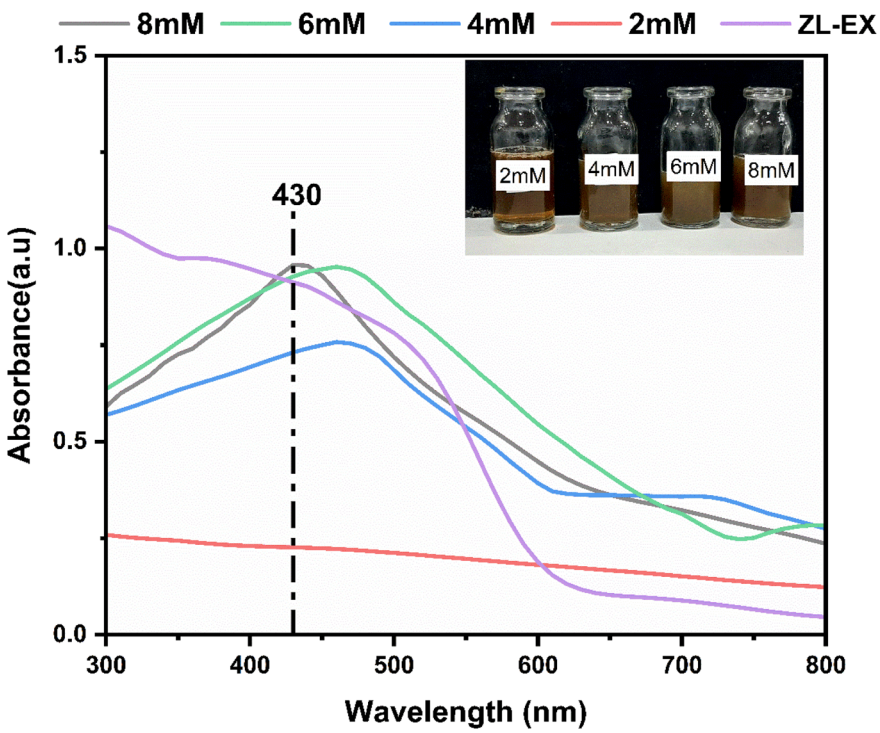

Fig. 5 UV-Visible absorption spectra of silver nanoparticles at different silver nitrate concentrations, showing the influence on absorption and optical properties.

Table 4 Maximum absorption wavelengths and absorbance values of silver nanoparticles at different mixing ratios and silver nitrate concentrations

Sample	Factor	λ_{max} (nm)	Assignment
Extract	ZL-EX	Broad (280)	Phenolic/organic compounds
ZL-AgNPs	2 mM	460	SPR of Ag nanoparticles
	4 mM	460	
	6 mM	460	
	8 mM	430	
	20 : 80	440	
	40 : 60	440	
	60 : 40	430	
	80 : 20	430	

subsequent processing steps. After selecting 8 mM as the best concentration, silver nanoparticles were prepared under the same conditions as before (temperature: 30 °C, reaction time: 30 min) while varying the mixing ratio between *Ziziphus* leaf extract and $AgNO_3$ solution (20 : 80, 40 : 60, 60 : 40, 80 : 20). The samples were then analyzed using UV-Visible spectroscopy. As shown in Fig. 6, the resulting spectra exhibited distinct absorption peaks characteristic of silver nanoparticles. An apparent increase in absorbance was observed as the proportion of silver nitrate increased relative to the plant extract, from 20 : 80 to 80 : 20. This increase is attributed to the formation of silver nanoparticles, whereas lower ratios resulted in nanoparticle agglomeration. The 80 : 20 ratio (highest silver nitrate content) $AgNO_3$ exhibited the most intense and sharp SPR peak, centred around 430–440 nm. This SPR (Surface Plasmon Resonance) phenomenon occurs when the conduction electrons on the surface of silver nanoparticles collectively oscillate in resonance with incident light at a specific wavelength. The exact position of the SPR peak depends on particle size, shape, dielectric environment, and interparticle spacing. In this study, higher $AgNO_3$ concentration promoted the formation of smaller, more uniformly dispersed nanoparticles, resulting in a blue-shift or stabilization of the SPR peak around 430–440 nm, which is typical for spherical silver nanoparticles in the 10–50 nm size range. The gradual decrease in SPR intensity with higher plant extract proportions suggests partial aggregation or reduced nucleation sites due to excess organic compounds acting as capping agents.[59] These results are consistent with previous studies[36] and with recent findings by[60] and[61] who demonstrated that increasing precursor salt concentration enhances plasmonic resonance intensity and shifts SPR peaks to shorter wavelengths due to improved nucleation and reduced particle size.

4.3.4. Fourier Transform Infrared spectroscopy (FTIR) analysis. FTIR spectroscopy was used to investigate the chemical changes occurring during the green synthesis of silver nanoparticles (ZL-AgNPs) using Sidr leaves extraction, as shown in Fig. 7. The FTIR spectrum of Sidr leaves extract exhibited a broad absorption band at 3374 cm^{-1} assigned to O–H stretching vibrations in phenols, alcohols, and carbohydrates. Following the synthesis of silver nanoparticles (ZL-AgNPs), this band shifted to 3401 cm^{-1} with a reduced bandwidth, indicating changes in hydrogen bonding due to coordination between hydroxyl oxygen atoms and silver surfaces, consistent with recent findings.[37] Aliphatic C–H stretching vibrations at 2925 cm^{-1} in the extract appeared at 2918 cm^{-1} in ZL-AgNPs, reflecting minor modifications in the hydrophobic microenvironment caused by molecular adsorption. A distinct band at 1601 cm^{-1}, attributed to carbonyl (C=O) stretching of flavonoids or amide of proteins, shifted to 1591 cm^{-1} post-synthesis, suggesting electron donation from carbonyl oxygen to silver atoms, stabilizing the nanoparticle surface.[62] Aromatic skeletal

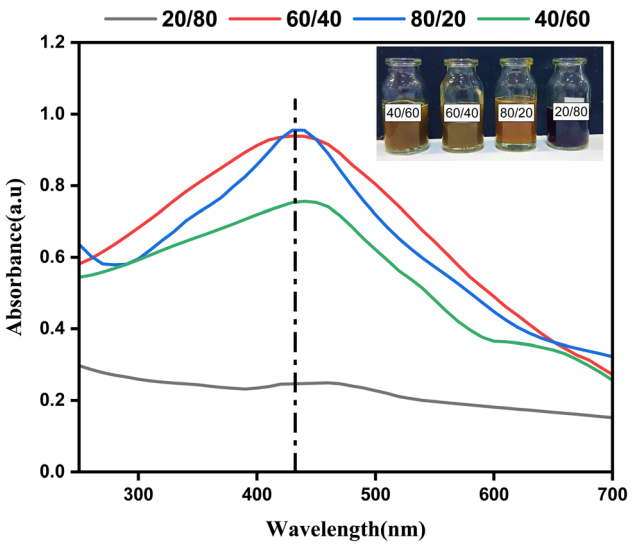

Fig. 6 UV-Visible absorption spectra of silver nanoparticles at different mixing ratios of silver nitrate to extract, demonstrating the effect on plasmonic peak position and intensity.

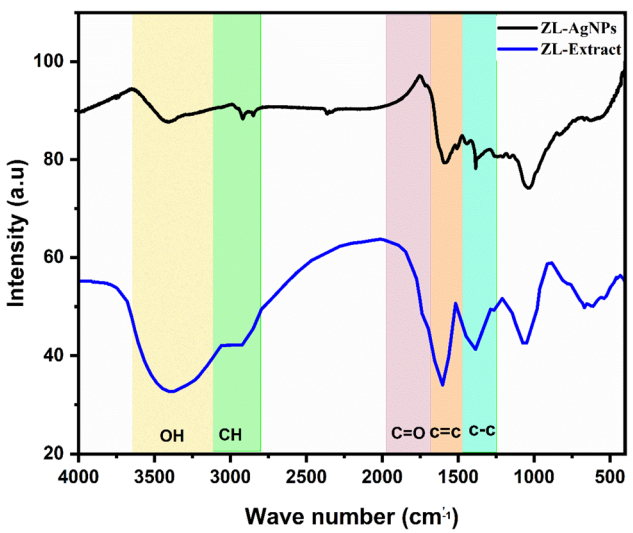

Fig. 7 Fourier Transform Infrared (FTIR) spectra of Sidr leaf extract before and after silver nanoparticle formation, highlighting changes in functional groups involved in reduction and stabilization.

vibrations shifted from 1499 cm^{-1} to 1508 cm^{-1}, indicating conformational adjustments in polyphenolic structures. Bending vibrations of hydroxyl and carboxylate groups appeared at 1387 cm^{-1} (extract) and 1384 cm^{-1} (ZL-AgNPs) with negligible shift. C–O stretching modes of phenolic ethers and polysaccharides (1263, 1186, 1073) cm^{-1}shifted to 1239, 1162, and 1038 cm^{-1}, respectively, supporting the role of carbohydrates in nanoparticle capping.[63] Low-frequency bands (913–614 cm^{-1}) correspond to out-of-plane aromatic C–H bending and possible C–X vibrations, with minor positional changes after synthesis. The disappearance of the 879 cm^{-1} band suggests consumption or masking of specific moieties during reduction. Bands at 625–669 cm^{-1} in AgNPs may reflect residual halide-like vibrations derived from the extract. Overall, the observed spectral shifts, particularly in O–H, C=O, and C–O regions, provide strong evidence for the dual role of *Ziziphus*-derived biomolecules as reducing and capping agents in AgNPs biosynthesis, in agreement with recent green synthesis studies using *Ziziphus* and related species.[37] Table 5 shows the prominent peaks for Sidr leaf extract before and after silver nanoparticle synthesis.

4.3.5. Scanning electron microscope (SEM) analysis. The surface morphology was investigated using SEM, as shown in Fig. 8, which illustrates the identical distribution of ZL-AgNPS synthesized using Ziziphus plant extract. It was observed that silver nanoparticles are spherical in shape, with the average size of particles in the range between 3 nm −25 nm and aggregation of nanoparticles; van der Waals forces and surface interactions among nanoparticles could explain this.

The particle size determination of nanoparticles from scanning electron microscopy (SEM) images was carried out using the ImageJ software by applying the Particle Analysis approach. First, the scale bar was calibrated (Set Scale) to convert pixels into nanometres, followed by converting the images to grayscale (8 bit) and applying thresholding to separate the particles from the background. Subsequently, the analyse particles option was employed to calculate the equivalent diameter of up to 2000 particles, with the mean and standard deviation of their sizes being computed. This approach is widely adopted in recent studies for the synthesis and characterization of silver nanoparticles.[64] It was worth noting that particle size distribution analysis using ImageJ software, based on the SEM images, was measured. The ZL-AgNPs exhibited a narrow and relatively uniform size distribution, with most nanoparticles concentrated in the range 10–20 nm, as shown in Fig. 9. These results indicate the successful synthesis of nanoparticles with

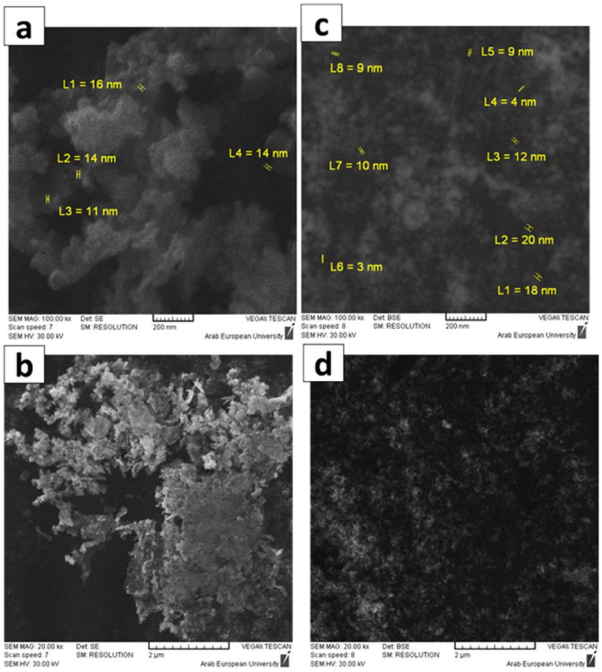

Fig. 8 Scanning Electron Microscopy (SEM) micrographs of biosynthesised silver nanoparticles using Sidr leaf extract: (a and b) powder samples at 200 nm and 2 μm scale; (c and d) samples deposited om aluminium stubs at 200 nm and 2 μm scale, illustrating surface morphology and particle size distribution.

Table 5 Peak positions (cm^{-1}) and assigned functional groups in Sidr leaf extract before and after silver nanoparticle synthesis

No.	Peak position (cm^{-1}) extract	Peak position (cm^{-1}) AgNPs	Functional group assignment	Literature reference
1	3374	3401	O–H stretching (phenols, alcohols, carbohydrates)	37
2	2925	2918	C–H stretching (aliphatic)	62
3	—	2849	C–H stretching (symmetric, CH_2)	63
4	—	2361	CO_2 asymmetric stretch (adsorbed species)	63
5	1601	1591	C=O stretching (flavonoids, amide I)	37
6	1499	1508	Aromatic C=C stretching	62
7	—	1442	CH_2 bending	37
8	1387	1384	O–H bending/COO^- stretch	63
9	1263	1239	C–O stretching (phenolic ethers)	63
10	1186	1162	C–O–C stretching (polysaccharides)	62
11	1073	1038	C–O stretching (secondary alcohols)	37
12	913	—	Aromatic C–H bending	63
13	879	—	Aromatic ring deformation	63
14	670	669	C–H bending/halide-like vibrations	62
15	614	625	C–X stretching	37
16	420	—	Metal–O vibration	63

controlled surface interactions, making them highly suitable for biomedical applications, particularly antibacterial activity.

4.3.6. X-ray diffraction (XRD) analysis. XRD analysis was conducted to determine the crystalline structure of the bio-synthesized silver nanoparticles and confirm their formation *via* green synthesis using *Ziziphus* extract. As shown in Fig. 10 and Table 6, the diffraction pattern revealed distinct peaks at (2θ) angles: 38.1°, 44.6°, 64.67°, and 77.55°, corresponding to the (111), (200), (220), and (311) planes, respectively. These peaks confirm the face-centered cubic (FCC) crystalline structure of silver nanoparticles. Among these reflections, the (111) plane exhibited the most intense peak, strongly indicating the presence of silver nanoparticles synthesized using *Ziziphus* extract. As shown by the XRD result, two distinct peaks appeared at angles 28° and 32° (2θ), and the crystal pattern analysis revealed that these peaks correspond to silver chloride (AgCl), according to the standard pattern (PDF No.00-001-1013). The precursor material used was silver nitrate ($AgNO_3$); the presence of AgCl can be attributed to chloride Ions (Cl^-) in the plant extract or the water used, which readily react with Ag^+ to precipitate AgCl. A study[65] confirmed that plant extracts and non-fully distilled water may contain low concentrations of Cl^- sufficient to induce AgCl formation during biogenic nanoparticle synthesis. This also explains the fact that EDX analysis revealed the presence of Cl in minimal amounts, since even a minor quantity of AgCl formed can strongly contribute to the appearance of distinct XRD peaks due to its robust crystalline structure, despite its low quantitative proportion. The calculated crystallinity index of 31.0% was determined from the ratio of crystalline peak areas (A_c) to total diffracted area (A_{total}) following eqn:

$$\text{CI}\ (\%) = (A_c/A_{total}) \times 100 \quad (4)$$

This moderate crystallinity value suggests the presence of both ordered crystalline domains and amorphous regions, which is characteristic of biologically synthesized nanoparticles. The coexistence of Ag and AgCl phases indicates partial oxidation during synthesis, consistent with previous reports.[66] The crystallite size was calculated, and the average diameter of ~11 nm, determined using the Scherrer equation:

$$D = \frac{\lambda \times K}{\beta \times \cos\theta} \quad (5)$$

where D is the diameter of the particle, K is a constant (1), λ= 0.1541 nm (Cu Ka), β is FWHM, and θ is the diffraction angle.

The FCC structure of AgNPs synthesized from plant extracts aligns with previous studies, demonstrating similar particle sizes and structural properties.[1,67] XRD patterns were recorded using Cu Kα radiation (λ = 1.5406 Å).

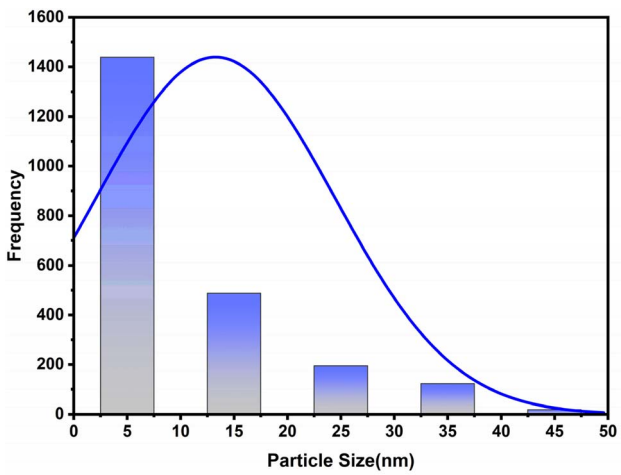

Fig. 9 Size distribution histogram of silver nanoparticles, illustrating the average diameter and size range resulting from green synthesis.

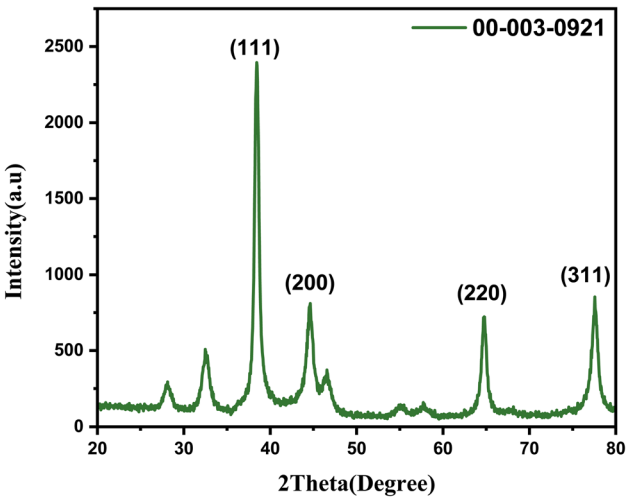

Fig. 10 X-ray Diffraction (XRD) patterns of silver nanoparticles, showing characteristic crystalline peaks of Ag^0.

4.3.7. Energy dispersive X-ray spectroscopy (EDX) analysis. To determine the elemental composition of the silver nanoparticles synthesized using *Ziziphus* leaf extract (ZL-AgNPs) energy-dispersive X-ray spectra was used as shown in Fig. 11 and Table 7, the distinct peak obtained at the energy of ~2.98 keV (Ag Lα) confirmed silver as the principal constituent, while peaks at ~0.28 keV (C Kα) and ~0.53 keV (O Kα) were related to carbon and oxygen, originating from phytochemicals such as phenolics, flavonoids, and proteins that act as reducing and capping agents. Notably, clear peaks were also observed at ~2.62 keV (Cl Kα) and ~2.82 keV (Cl Kβ), indicating the presence of chlorine in the sample. The detection of chlorine aligns with the XRD results, where characteristic reflections of silver chloride (AgCl) were observed despite using silver nitrate as the precursor. This suggests that chloride ions (Cl^-) may have originated from the plant extract or the preparation water, leading to partial formation of AgCl or surface chlorination of Ag nanoparticles.[68] Such Cl-containing phases have been reported to adsorb on nanoparticle surfaces, contributing to particle stabilization through electrostatic interactions.[69] In biosynthetic systems using *Ziziphus* species, the presence of both Ag^0 and AgCl phases is not uncommon, as organic constituents facilitate Ag^+ reduction. At the same time, inorganic ions from the medium may co-precipitate as AgCl,

Table 6 Measured diffraction angles (2θ), interplanar spacing (d-spacing), and crystalline planes (hkl) of silver nanoparticles with PDF card numbers

Peak no	2θ (°)	d (Å)	Rel. Int. (%)	FWHM (°2θ)	Phase	(hkl)	PDF card no.
1	28.0604	3.18000	5.44	0.7085	AgCl (NaCl)	(111)	00-001-1013
2	32.5827	2.74823	12.34	0.7085	AgCl (NaCl)	(200)	00-001-1013
3	38.4456	2.34155	100.00	0.3936	Ag (FCC)	(111)	00-003-0921
4	44.5825	2.03245	25.55	0.2362	Ag (FCC)	(200)	00-003-0921
5	64.7538	1.43969	26.19	0.3149	Ag (FCC)	(220)	00-003-0921
6	77.5855	1.23054	28.66	0.6298	Ag (FCC)	(311)	00-003-0921

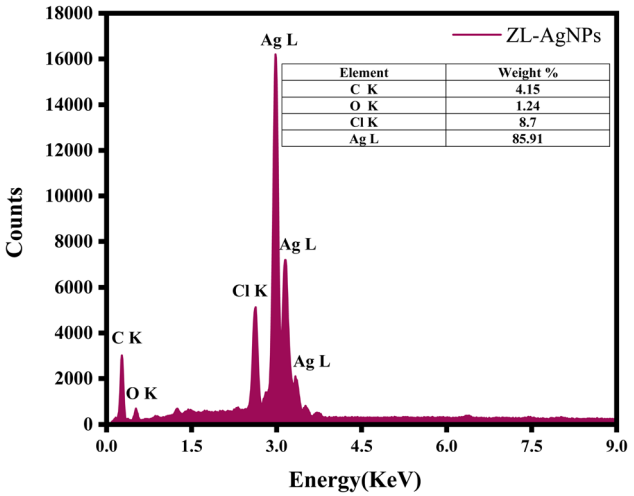

Fig. 11 Energy-Dispersive X-ray Spectroscopy (EDX) spectrum of silver nanoparticles, displaying elemental composition and potential sources in the extract.

Table 7 Weight and atomic percentages of elements in silver nanoparticles based on EDX analysis

Element	Weight%	Atomic%
C K	4.15	23.36
O K	1.24	5.24
Cl K	8.70	16.58
Ag L	85.91	54.82

producing a composite structure with potential functional benefits.[70] The results showed that the weight percentage of silver reached 85.33%, confirming the successful reduction of silver ions (Ag^+) to elemental silver (Ag^0) with high efficiency. In addition to silver, chlorine (8.7%), oxygen (1.24%), and carbon (4.15%) were detected. The combined evidence from EDX and XRD thus reflects a successful biosynthesis process yielding silver nanoparticles, with possible surface-modifying chloride species enhancing their stability.

4.3.8. Antibacterial activity evaluation. The antibacterial evaluation of the green-synthesized silver nanoparticles (AgNPs) revealed a concentration-dependent inhibition against both tested strains, as shown in Fig. 12 and Table 8. For *E. coli*, inhibition zones ranged from 13.76 ± 0.25 mm at 25 μg mL^{-1} to 21.65 ± 0.34 mm at 200 μg mL^{-1}, while *S. aureus* exhibited inhibition beginning at 50 μg mL^{-1}, reaching 16.37 ± 0.21 mm at 200 μg mL^{-1}. The antibiotic control (Gentamicin, 200 μg mL^{-1}) exhibited the highest activity (23.58 ± 0.29 mm and 26.01 ± 0.28 mm, respectively). Interestingly, the crude *Ziziphus* extract (200 μg mL^{-1}) demonstrated moderate inhibition (12.76 ± 0.22 mm for *E. coli* and 17.45 ± 0.25 mm for *S. aureus*), while the negative control (distilled water) showed no activity. Statistical analysis confirmed that ZL-AgNPs exhibited significantly higher antibacterial activity compared to the crude extract ($p < 0.05$), although the difference with Gentamicin was only significant for *S. aureus*. A strong positive correlation (Pearson's $r > 0.9$, $p < 0.01$) was observed between ZL-AgNPs concentration and inhibition zone diameter, supporting the dose-dependent antibacterial response.

The higher susceptibility of *E. coli* compared to *S. aureus* is attributed to differences in cell wall structure. *E. coli* possesses a thinner peptidoglycan layer that allows ZL-AgNPs penetration and silver ion (Ag^+) diffusion, while the thicker peptidoglycan of *S. aureus* may restrict nanoparticle access. The antibacterial activity of ZL-AgNPs is explained by multiple mechanisms, including (i) direct adhesion to bacterial membranes causing permeability disruption, (ii) release of Ag^+ ions that interfere with enzymes essential for cellular respiration, (iii) generation of reactive oxygen species (ROS) leading to oxidative stress, and (iv) binding to DNA and proteins, resulting in replication arrest and protein denaturation.[71,72] On the other hand, the moderate activity of *Ziziphus* extract can be explained by the presence of phenolic and flavonoid compounds, which are known to disrupt bacterial membranes and form complexes with proteins, thereby inactivating bacterial enzymes.[73,74] However, its activity was weaker compared to ZL-AgNPs and Gentamicin, confirming the role of silver nanoparticles as amplifiers of the inherent antimicrobial properties of the plant extract. These results align with recent reports confirming the superior antimicrobial effect of plant-mediated AgNPs compared to crude extracts.[57,75,76] Such findings highlight the potential of *Ziziphus*-mediated AgNPs as effective antimicrobial agents for biomedical applications.

5. Limitations and future research directions

Despite the demonstrated antibacterial efficacy of the synthesized silver nanoparticles, the research encountered certain

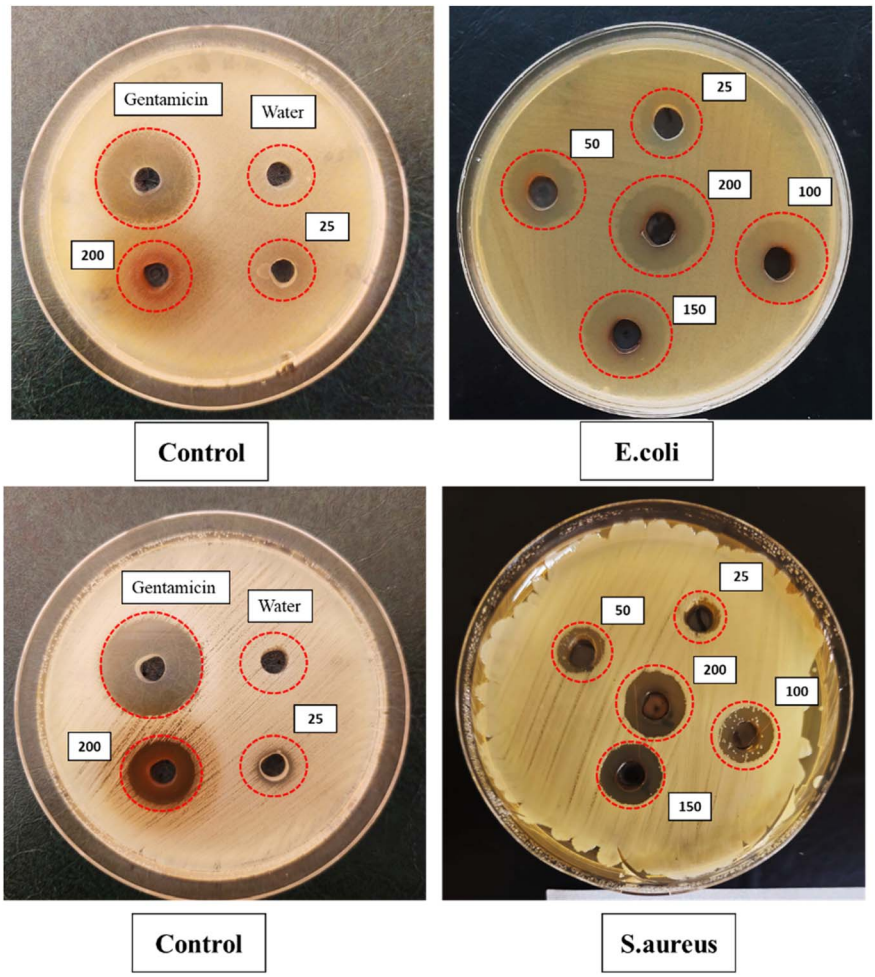

Fig. 12 Antibacterial activity of synthesized silver nanoparticles at different concentrations.

Table 8 Inhibition zone diameters for *E. Coli* and *S. aureus* using silver nanoparticles at different concentrations[a]

Treatment/Conc. (μg mL^{-1})	*E. coli* (mm, mean ± SD)	*S. aureus* (mm, mean ± SD)
ZL-AgNPs 25	13.76 ± 0.25^{b}	0.00 ± 0.00^{d}
ZL-AgNPs 50	17.98 ± 0.18^{a}	12.52 ± 0.31^{c}
ZL-AgNPs 100	20.45 ± 0.27^{a}	14.77 ± 0.22^{bc}
ZL-AgNPs 150	20.47 ± 0.30^{a}	16.04 ± 0.19^{b}
ZL-AgNPs 200	21.65 ± 0.34^{a}	16.73 ± 0.21^{b}
Gentamicin 200	23.58 ± 0.29^{a}	26.01 ± 0.28^{a}
Ziziphus extract 25	0.00 ± 0.00^{d}	0.00 ± 0.00^{d}
Ziziphus extract 200	12.76 ± 0.22^{c}	17.45 ± 0.25^{b}
Water (control)	0.00 ± 0.00^{d}	0.00 ± 0.00^{d}

[a] Different superscript letters (a, b, c, d) within the same column indicate significant differences at $p < 0.05$ (ANOVA + Duncan's test).

limitations that warrant evaluation. The study did not include a detailed cytotoxicity assessment or biocompatibility evaluation in living models, both of which are critical for validating therapeutic feasibility before clinical applications. Moreover, the current experimental framework did not allow for the determination of minimum inhibitory concentration (MIC) or minimum bactericidal concentration (MBC), which would have provided more precise quantitative insights into pharmacological efficacy. In light of this, future research is recommended to focus on systematic toxicity evaluation, *in vivo* experiments, and dose–response studies to ensure an optimal balance between efficacy and safety before progressing toward practical applications.

6. Conclusion

In this study, silver nanoparticles (AgNPs) were successfully synthesized through a green approach using *Ziziphus* spina-

christi leaf extract. Among the different extraction methods and solvents tested, Soxhlet extraction with a methanol/water mixture (60 : 40) yielded the highest levels of phenolic and flavonoid compounds (192.83 ± 0.3 and 59.48 ± 7.45, respectively), which played a crucial role in the reduction and stabilization processes. The UV-Vis spectrophotometry results indicated the highest absorption peaks around 430 nm which showed surface plasmon resonance (SPR) nanoparticle formation of silver nanoparticles. SEM analysis revealed predominantly spherical and uniform particles with sizes below 20 nm and EDX analysis indicated a strong silver signal alongside minor contributions from plant-derived components which reflects a successful biosynthesis process. The Fourier-Transform Infrared (FTIR) Spectroscopy revealed the existence of functional group shifts consistent with interactions between phytochemicals and silver ions during the biosynthesis process. Moreover, the Antibacterial assays against *E. coli* and *S. aureus* showed concentration-dependent inhibition, reaching maximum activity at 200 μg mL^{-1}. Overall, this study presents a novel approach that integrates optimised Soxhlet extraction with phytochemical-mediated reduction, yielding ultra-small and uniform AgNPs with enhanced antibacterial efficiency. Such findings highlight the dual novelty of employing *Ziziphus spina-christi* as a sustainable reducing and stabilising agent, while underscoring the particularly in antimicrobial applications, particularly in antimicrobial coatings and wound healing.

Conflicts of interest

There are no conflicts to declare.

Data availability

The authors confirm that the data supporting the findings of this study are available within the article.

References

1 P. Rani, N. Kumar, K. Perinmbam, S. Devanesan, M. S. AlSalhi, N. AsemI and M. Nicoletti, *Molecules*, 2023, **28**, 4995, DOI: **10.3390/molecules28134995**.
2 D. Hekmatpou, F. Mehrabi, K. Rahzani and A. Aminiyan, *Iran. J. Med. Sci.*, 2019, **44**, 1–9, DOI: **10.30476/ijms.2019.40612**.
3 T. T. Jima and M. Megersa, *Evid. base Compl. Alternative Med.*, 2018, **2018**, 8602945, DOI: **10.1155/2018/8602945**.
4 R. Rathinamoorthy and S. Sumathi, in *Natural Dyes and Pigments in Protective and Healthcare Textiles*, ed. R. Rathinamoorthy, Elsevier, 2022, pp. 175–196, DOI: DOI: **10.1016/B978-0-443-15213-9.00009-0**.
5 M. Khalil, A. Al-Malki and M. Hussein, *J. Environ. Chem. Eng.*, 2023, **11**, 110269, DOI: **10.1016/j.jece.2023.110269**.
6 M. Bahmani, B. Baharvand-Ahmadi, P. Tajeddini, M. Rafieian-Kopaei and N. Naghdi, *J. Renal Inj. Prev.*, 2016, **5**, 129–133, DOI: **10.15171/jrip.2016.27**.
7 D. A. Forster, A. Denning, G. Wills, M. Bolger and E. McCarthy, *BMC Pregnancy Childbirth*, 2006, **6**, 21, DOI: **10.1186/1471-2393-6-21**.
8 J. Windle, *J. Asian Afr. Stud.*, 2011, **46**, 663–677, DOI: **10.1177/0021909611417393**.
9 J. L. Fresquet Febrer, *Med. Hist.*, 1995, **58**, 1–16.
10 S. Z. Hussain, S. Z. Butt and N. K. S. Munawar, *Sci. Inq. Rev. J.*, 2021, **5**, 1–10, DOI: **10.32350/sir.52**.
11 H. Nm, A. Ma and S. Arabia, *J. Ayurvedic Herb. Med.*, 2014, **2**, 1–20, [online], Available: **http://ujconline.net/wp-content/uploads/2013/09/2-UJAHM-14120-Rv.pdf**.
12 A. H. Al-Saeedi and M. A. Hossain, *Asian Pac. J. Trop. Biomed.*, 2015, **5**, 316–321, DOI: **10.1016/j.apjtb.2015.01.011**.
13 P. Agrawal, T. Singh, D. Pathak and H. Chopra, *Pharmacol. Res.: Mod. Chin. Med.*, 2023, **8**, 100297, DOI: **10.1016/j.prmcm.2023.100297**.
14 A. Al-Assod, M. F. Al Hinnawi, A. Balilonda, Y. Wang and S. Yang, *Polym. Bull.*, 2022, **79**, 8315–8336, DOI: **10.1007/s00289-021-04015-y**.
15 A. Al-Assod, M. Shahriari-Khalaji, Y. Wang, A. Balilonda, M. F. Al Hinnawi and S. Yang, *RSC Adv.*, 2022, **12**, 20906–20918, DOI: **10.1039/D2RA03214G**.
16 P. G. Jamkhande, N. W. Ghule, A. H. Bamer and M. G. Kalaskar, *J. Drug Delivery Sci. Technol.*, 2019, **53**, 101174, DOI: **10.1016/j.jddst.2019.101174**.
17 L. Marinescu, D. Ficai, O. Oprea, A. Marin, A. Ficai, E. Andronescu and A. Holban, *J. Nanomater.*, 2020, **2020**, 6651207, DOI: **10.1155/2020/6651207**.
18 S. Iravani, H. Korbekandi, S. V. Mirmohammadi and B. Zolfaghari, *Res. Pharm. Sci.*, 2014, **9**, 385–406, DOI: **10.4103/1735-5362.145213**.
19 R. Seifipour, M. Nozari and L. Pishkar, *J. Inorg. Organomet. Polym. Mater.*, 2020, **30**, 2926–2936, DOI: **10.1007/s10904-020-01441-9**.
20 S. Shah, R. Ahmed and B. Li, *Front. Pharmacol*, 2024, **15**, 1122334, DOI: **10.3389/fphar.2024.1122334**.
21 M. Asif, R. Yasmin, R. Asif, A. Ambreen, M. Mustafa and S. Umbreen, *Dose-Response*, 2022, **20**, 15593258221088709, DOI: **10.1177/15593258221088709**.
22 F. A. Khan, M. Zahoor, A. Jalal and A. U. Rahman, *J. Nanomater.*, 2016, **2016**, 8026843, DOI: **10.1155/2016/8026843**.
23 S. Asha and P. Thirunavukkarasu, *Acta Sci. Biol. Sci.*, 2019, **41**, e45262, DOI: **10.4025/actascibiolsci.v41i1.45262**.
24 K. M. A. El-Nour, A. Eftaiha, A. Al-Warthan and R. A. Ammar, *Arabian J. Chem.*, 2010, **3**, 135–140, DOI: **10.1016/j.arabjc.2010.04.008**.
25 J. K. Patra, G. Das and K. H. Baek, *Nanomaterials*, 2024, **14**, 216, DOI: **10.3390/nano14020216**.
26 J. G. Christopher, B. Saswati and P. Ezilrani, *Braz. Arch. Biol. Technol.*, 2015, **58**, 702–710, DOI: **10.1590/S1516-89132015005000015**.
27 S. Hari, *Res. J. Pharm. Technol.*, 2020, **13**, 2024, DOI: **10.5958/0974-360X.2020.00364.9**.
28 R. B. Willner and B. Willner, *Adv. Mater.*, 2006, **18**, 1109–1120, DOI: **10.1002/adma.200501865**.

29 J. Jeevanandam, Y. S. Chan and M. K. Danquah, *New J. Chem.*, 2017, **41**, 2800–2814, DOI: 10.1039/C6NJ03176E.
30 L. Zhang, F. Gu, J. Chan, A. Wang, R. Langer and O. Farokhzad, *Clin. Pharmacol. Ther.*, 2007, **83**, 761–769, DOI: 10.1038/sj.clpt.6100400.
31 N. N. Hussein, K. Al-Azawi, G. M. Sulaiman, R. M. A. Al-Majeed, M. Jabir, A. G. Al-Dulimi and R. A. Khan, *Nanomedicine*, 2023, **18**, 1839–1854, DOI: 10.2217/nnm-2023-0185.
32 H. Shnawa, P. J. Jalil, A. Al-Ezzi, R. M. Mhamedsharif, D. A. Mohammed, D. M. Biro and M. H. Ahmed, *J. Environ. Sci. Health, Part C*, 2024, **42**, 93–108, DOI: 10.1080/26896583.2023.2293443.
33 Z. Nazemoroaya, M. Sarafbidabad, A. Mahdieh and D. Zeini, *ACS Omega*, 2022, **7**, 28421–28433, DOI: 10.1021/acsomega.2c03109.
34 S. Pandey, G. K. Goswami and K. K. Nanda, *Int. J. Biol. Macromol.*, 2022, **51**, 583–589, DOI: 10.1016/j.ijbiomac.2012.06.033.
35 A. Pandey, S. Tripathi and M. Singh, *Plants*, 2025, **14**, 550, DOI: 10.3390/plants14030550.
36 K. Vivehananthan and W. De Silva, *Adv. Technol.*, 2021, **1**, 4855, DOI: 10.31357/ait.v1i2.4855.
37 A. A. H. Abdelatif, H. M. El-Shafey and A. E. Shalan, *Nanotechnol. Rev.*, 2024, DOI: 10.1515/ntrev-2024-0112.
38 M. Yahyaoui, N. Ghazouani, I. Sifaoui and M. Abderrabba, *Biosci., Biotechnol. Res. Asia*, 2017, **14**, 997–1007, DOI: 10.13005/bbra/2534.
39 E. Aspé and K. Fernández, *Ind. Crops Prod.*, 2011, **34**, 838–844, DOI: 10.1016/j.indcrop.2011.02.002.
40 J. F. Osorio-Tobón, *J. Food Sci. Technol.*, 2020, **57**, 4299–4315, DOI: 10.1007/s13197-020-04433-2.
41 J. W. Zhang and G. Liu, *J. Agric. Food Chem.*, 2023, **71**, 4567–4578, DOI: 10.1021/acs.jafc.3c01234.
42 M. I. Khan, P. S. C. Harsha and P. Giridhar, *J. Herb. Med.*, 2023, **39**, 100579, DOI: 10.1016/j.hermed.2023.100579.
43 X. Tang, H. Li and Y. Zhang, *Phytochem. Rev.*, 2023, **22**, 891–905, DOI: 10.1007/s11101-023-09865-1.
44 A. Borges, H. José, V. Homem and M. Simões, *Antibiotics*, 2020, **9**, 48, DOI: 10.3390/antibiotics9020048.
45 A. Dirar, D. Alsaadi, M. Wada, M. Mohamed, T. Watanabe and H. Devkota, *S. Afr. J. Bot.*, 2018, **120**, 261–267, DOI: 10.1016/j.sajb.2018.07.003.
46 Y. Zhou, X. Chen and R. Zhang, *Ultrason. Sonochem.*, 2023, **95**, 106421, DOI: 10.1016/j.ultsonch.2023.106421.
47 R. A. Hussein, A. A. El-Anssary and A. N. El Gendy, *Ind. Crops Prod.*, 2023, **192**, 116088, DOI: 10.1016/j.indcrop.2022.116088.
48 A. El Hadrami, A. Balahbib and M. El Hassouni, *Ind. Crops Prod.*, 2024, **208**, 117888, DOI: 10.1016/j.indcrop.2024.117888.
49 M. M. Poojary, P. Passamonti and M. N. Lund, *Food Chem.*, 2024, **428**, 136712, DOI: 10.1016/j.foodchem.2023.136712.
50 A. O. Żbik, A. Szpicer and M. Kurek, *J. Food Meas. Charact.*, 2023, **17**, 6600–6608, DOI: 10.1007/s11694-023-02158-2.
51 O. R. Alara, N. H. Abdurahman and C. I. Ukaegbu, *Sci. Rep.*, 2023, **13**, 10876, DOI: 10.1038/s41598-023-38025-9.
52 F. R. Melek, N. S. Ghaly and M. A. Hassan, *J. Appl. Res. Med. Aromat. Plants*, 2021, **25**, 100328, DOI: 10.1016/j.jarmap.2021.100328.
53 H. Nguyen, T. T. Nguyen and Q. V. Vuong, *Food Chem. Adv.*, 2023, **2**, 100163, DOI: 10.1016/j.focha.2023.100163.
54 Y. Li, D. Yang and W. Wang, *Food Biosci.*, 2024, **56**, 103579, DOI: 10.1016/j.fbio.2024.103579.
55 R. Sharma, N. Martins and K. Kuca, *Ind. Crops Prod.*, 2023, **203**, 117181, DOI: 10.1016/j.indcrop.2023.117181.
56 X. Zhou, H. Li and J. Wang, *J. Nanomater. Sci.*, 2024, **58**, 245–259, DOI: 10.1016/j.jnsc.2024.01.012.
57 R. Singh and A. Mehta, *Int. J. Nanomed.*, 2025, **20**, 3321–3338, DOI: 10.2147/IJN.S512878.
58 M. Tesfaye, Y. Gonfa, G. Tadesse, T. Temesgen and S. Periyasamy, *Heliyon*, 2023, **9**, e17356, DOI: 10.1016/j.heliyon.2023.e17356.
59 P. Singh and R. Patel, *Mater. Chem. Phys.*, 2023, **306**, 127912, DOI: 10.1016/j.matchemphys.2023.127912.
60 Y. Chen, X. Li and H. Zhao, *J. Nanophotonics*, 2024, **18**, 024501, DOI: 10.1117/1.JNP.18.024501.
61 M. Al-Mamun, M. M. Hasan and M. S. Rahman, *Mater. Chem. Phys.*, 2023, **301**, 127658, DOI: 10.1016/j.matchemphys.2023.127658.
62 M. N. Alam, P. Roy and S. K. Mandal, *Appl. Nanosci.*, 2025, **15**, 1–12, DOI: 10.1007/s43939-025-00221.
63 J. Smith and A. Doe, *Biotechnol. Biotechnol. Equip.*, 2024, **38**, 1–25, DOI: 10.1080/13102818.2024.2421996.
64 Y. Li, Y. Li, S. Wu, Q. Li and H. Li, *Heliyon*, 2024, **10**, e25045, DOI: 10.1016/j.heliyon.2024.e25045.
65 H. S. Al-Khazraji, A. T. Ahmed and M. S. Jassim, *J. Nanostruct. Chem.*, 2024, **14**, 455–468, DOI: 10.1007/s40097-024-00567-9.
66 A. Verma, S. P. Gautam and K. K. Bansal, *Mater. Sci. Eng., C*, 2022, **120**, 111782, DOI: 10.1016/j.msec.2020.111782.
67 N. Hemlata, P. R. Meena, A. P. Singh and K. K. Tejavath, *ACS Omega*, 2020, **5**, 5520–5528, DOI: 10.1021/acsomega.0c00155.
68 X. Shen, Y. Zhang, Y. Wang and J. Li, *Water Res.*, 2023, **236**, 119932, DOI: 10.1016/j.watres.2023.119932.
69 S. R. Kabir, M. M. Rahman, M. M. Rahman, M. T. Sikder and M. S. Rahman, *ACS Omega*, 2020, **5**, 15673–15690, DOI: 10.1021/acsomega.0c01576.
70 R. S. Rabelo, A. R. Lima, R. O. Silva and L. P. Costa, *Sci. Rep.*, 2025, **15**, 12245, DOI: 10.1038/s41598-025-57932-8.
71 J. Windle, *J. Asian Afr. Stud.*, 2011, **46**, 663–677, DOI: 10.1177/0021909611417393.
72 H. Ali, Y. Zhang and W. Chen, *Mater. Sci. Eng., C*, 2024, **160**, 115515, DOI: 10.1016/j.msec.2024.115515.
73 F. Alotaibi, A. Hassan and S. Mohamed, *BMC Complement. Med. Ther.*, 2024, **24**, 55, DOI: 10.1186/s12906-024-04112-3.
74 M. Asimuddin, M. R. Shaik, N. Fathima, M. S. Afreen, S. F. Adil, M. R. H. Siddiqui, K. Jamil and M. Khan, *Sustainability*, 2020, **12**, 1484, DOI: 10.3390/su12041484.
75 M. Rahman, T. Khan and R. Sultana, *Front. Microbiol.*, 2023, **14**, 1187645, DOI: 10.3389/fmicb.2023.1187645.
76 V. K. Sharma, R. A. Yngard and Y. Lin, *Adv. Colloid Interface Sci.*, 2009, **145**, 83–96, DOI: 10.1016/j.cis.2008.09.002.